ACS APPLIED POLYMER MATERIALS

pubs.acs.org/acsapm

Article

Fabrication of Nanowalled Catalytically Self-Threaded Supramolecular Polyrotaxane Microcapsules Using Droplet Microfluidics

Elnaz Alizadeh-Haghighi,[#] Aisan Khaligh,[#] Ali Kalantarifard, Caglar Elbuken,[*] and Dönüs Tuncel[*]

Cite This: *ACS Appl. Polym. Mater.* 2022, 4, 4681−4688

Read Online

ACCESS | Metrics & More | Article Recommendations | Supporting Information

ABSTRACT: Micrometer-scale monodisperse droplets are produced to generate nanowalled supramolecular microcapsules using microfluidics for high reproducibility and high-throughput manipulation, efficient material consumption, and control over hierarchical structure, shape, and size. In this study, an optimized microfluidic droplet generation technique and a unique liquid−liquid interfacial polymerization method were applied to fabricate the monodisperse polyrotaxane−based supramolecular microcapsules in a fast and simple way. To minimize the uncertainty due to droplet volume variation, the inlet pressures were supplied from the same source while lowering the interfacial tension and the main channel hydrodynamic resistance, which are critical for high monodispersity. The target polyrotaxane network (PN) was simply formed at the interface of the water and oil phases in ultra-monodisperse microdroplets via the cucurbit[6]uril (CB6)-catalyzed azide−alkyne cycloaddition (CB6-AAC) reaction between azido- and alkyne-functionalized tetraphenylporphyrin monomers (TPP-4AZ and TPP-4AL). The thickness of the interfacially assembled PN microcapsules was 20 nm as analyzed by cross-sectional TEM and TEM-EDX techniques. The resultant water-in-oil PN microcapsules were highly monodisperse in size and able to retain target molecules. Here, rhodamine 6G (Rh6G)-loaded PN microcapsules were fabricated, and the release rate of the Rh6G cargo was investigated over time for controlled drug release applications.

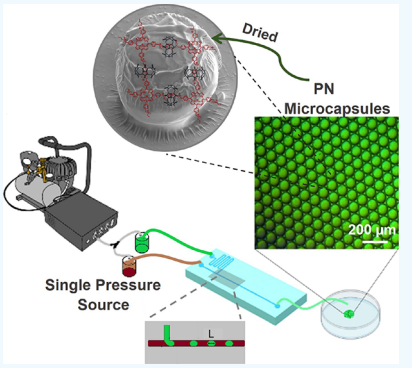

KEYWORDS: *microfluidics, nanowalled microcapsules, monodispersity, supramolecules, 2D polyrotaxane network, interfacial polymerization, drug release*

1. INTRODUCTION

Considerable attention has been devoted to the development of free-standing two-dimensional (2D) supramolecular assemblies as thin films for diverse applications such as biosensing and optoelectronics due to their unique properties and well-designed structures. Recently, liquid-to-liquid interfacial polymerization served as an efficient method that accommodates large-area, continuous, and free-standing 2D films at the interface of two liquid phases.[1,2] In comparison to planar interfaces, the spherical surface of these supramolecular assemblies in the form of microdroplets offers improved interaction with the surrounding environment for many applications.[3]

Porphyrin derivatives are one of the most attractive components for the fabrication of 2D supramolecular assemblies due to their synthetic versatility, facile modification, chemical stability and flexibility, planar structure, and rigidity as well as outstanding photo- and electrochemical properties. Owing to these unique properties, porphyrins have been widely used in the construction of rotaxane-based assemblies with cucurbit[*n*]urils,[4−7] in which the CB[*n*] macrocycle is threaded onto an axle-like component through noncovalent interactions. These engineered rotaxane assemblies offer many interesting properties and extensive applications especially in construction of stimuli-responsive materials.[8−16]

CB[*n*]s are a family of macrocyclic compounds composed of glycoluril units connected by methylene bridges. They offer strong host−guest chemistry owing to their rigid hydrophobic cavity and two identical hydrophilic carbonyl portals. They can be found in various sizes depending on the number of glycol units present in their structure.[13] CBs have become important building blocks of supramolecular assemblies because of their interesting structural features, which can provide rich host−guest chemistry as well as displaying outstanding properties such as nontoxicity, high biocompatibility, and thermal and chemical stability.[12,14−24] Among CBs, CB6 with six glycol units is unique due to its ability to catalyze 1,3-dipolar cycloaddition between properly substituted alkyne and azide

Received: January 30, 2022
Accepted: April 2, 2022
Published: April 11, 2022

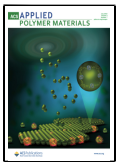

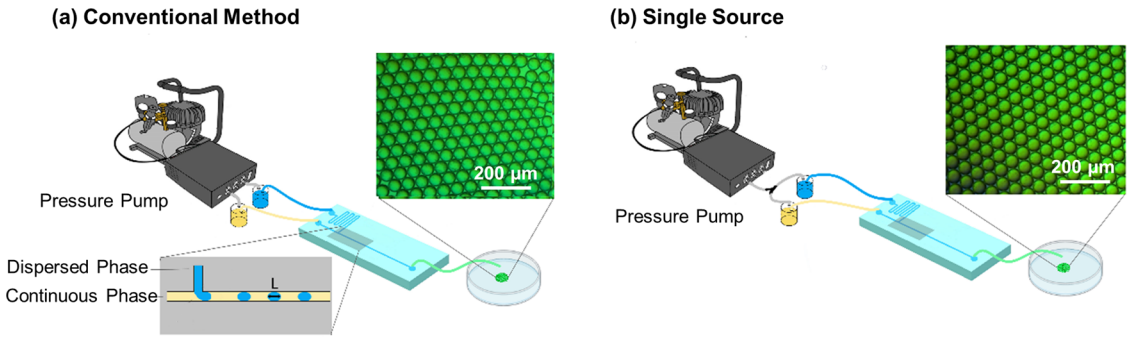

Figure 1. Schematic representation of the microfluidic system using (a) the conventional method, where the droplet generator driven by two ports on the pressure supply, and (b) the proposed single source method, where the droplet generator driven by connecting to a single port of the pressure supply.

substrates by forming 1,4-disubstituted triazoles. This feature was extensively explored in the synthesis of rotaxanes and polyrotaxanes.[1,6,9,22,23]

Thanks to their capability of encapsulation, adaptive dynamic, high specific surface area, and low effective density, microcapsules have favorable applications such as the production of artificial organelles, self-healing concrete, cosmetics, biomedical diagnostics, transport of vaccines, regenerative biomedicines, microreactor-targeted drug delivery, tissue engineering, adhesives, paints, pesticides, living cell-integrated assays, and magnetic devices and materials.[25−30] In this context, the hierarchically ordered supramolecular frameworks that are formed by the self-assembly of appropriate molecular building blocks could be applied to form self-adjusting microcapsules with stimuli responsiveness, tunable porosity, and stability.

Microfluidics is a powerful tool for the production of monodisperse microdroplets that can result in microcapsules with high-throughput generation, effective consumption of material, and high reproducibility along with precise control over hierarchical structure, shape, and size.[31] Microfluidic techniques applied for the generation of microcapsules have addressed issues such as the restricted efficiency of encapsulation and multiple steps of synthesis.[32] First, microfluidic microcapsule generation was demonstrated by Weitz et al.[33] Then, several techniques have been developed to achieve the microdroplet-based production of microcapsules.[29,33−35] Encapsulation is usually accomplished by single- or double-microdroplet emulsion generation. Subsequently, these microdroplets, which involve biopolymers, synthetic polymers, amphiphiles or lipids, endure the solidification of skin via polymerization, evaporation of solvent, or dewetting. To ensure the monodispersity of the generated microcapsules, it is essential to ensure that the volume variation of the primary droplets, which serve as microcapsule precursors, is minimized. To provide ultra-monodisperse droplet generation, internal and external factors that disturb monodispersity and the system dynamics should be investigated as we have shown in our previous work.[27,30,35−38]

During the past few years, limited studies have been reported on microcapsule generation via the combination of microfluidic techniques and CB-based supramolecular architectures. These microcapsules are primarily fabricated through the CBs' host−guest interactions using three methods: interfacial condensation-driven assembly, electrostatic interaction-driven assembly, and colloidal particle-driven assembly.[3,31,39−41] Combining the advantages of microfluidic droplets and supramolecular chemistry, the fabrication of stable CB-based supramolecular microcapsules in an efficient and simple process is still challenging.

Recently, we have reported the synthesis of a catalytically self-threaded 2D polyrotaxane network (PN) through a facile water−oil interfacial polymerization method between tetra-azide- and tetra-alkyne-functionalized porphyrins, in which CB6 catalyzed the azide−alkyne cycloaddition reaction (CB6-AAC) between two porphyrin monomers, and therefore, the polymerization and rotaxane formation occurred simultaneously at the interface.[1] PN film was successfully utilized as an efficient photosensitizer for antibacterial photodynamic therapy.[1] In this work, we demonstrate the versatility and adaptability of this approach in the direct construction of ultra-monodisperse and stable PN microcapsules in a single step using an optimized microfluidic droplet generation technique. PN as the microdroplet shell was formed through the interfacial polymerization between the aqueous and the oil phases containing TPP-4AZ, CB6, and TPP-4AL, respectively. Here, CB6 fosters the catalytic self-assembly of two functionalized porphyrin monomers at the interface of water and oil in ultra-monodisperse droplets. To the best of our knowledge, this is the first example of catalytically self-threaded polyrotaxane network microcapsules fabricated through CB6-promoted click chemistry.

2. EXPERIMENTAL SECTION

2.1. Materials and Instrumentation. All chemicals and reagents used in this work were of analytical grade and purchased from Sigma-Aldrich. Ultrapure deionized water ($R \geq 18$ MΩ cm^{-1}) from a Milli-Q plus (Millipore, Bedford, MA, USA) water purification system was used to prepare all aqueous solutions. CB6, the porphyrin monomers (TPP-4AZ and TPP-4AL), and the target PN were synthesized and fully characterized according to the procedures presented in our earlier paper.[1]

Scanning electron microscopy (SEM) images were captured by a SEM-FIB instrument (FEI NovaLab 600i). Focused ion beam (FIB) milling was used to obtain the cross-sectional images of PN microcapsules as well as to prepare a thin film of PN microcapsule layers for TEM cross-sectional inspections. The area of interest was protected with the deposition of 1 μm of platinum before etching. Transmission electron microscopy (TEM) images and energy-dispersive X-ray spectroscopy (EDX) analysis were acquired by FEI Tecnai G2 F30 TEM. Confocal laser scanning microscopy (CLSM) images were taken by Leica TCS SP8 X multiphoton system in fluorescence mode with the excitation laser at 490 nm, intensity of 80%, and emission range of 608−749 nm. Transmission and fluorescence images of the microcapsules were obtained using a

https://doi.org/10.1021/acsapm.2c00195
ACS Appl. Polym. Mater. 2022, 4, 4681−4688

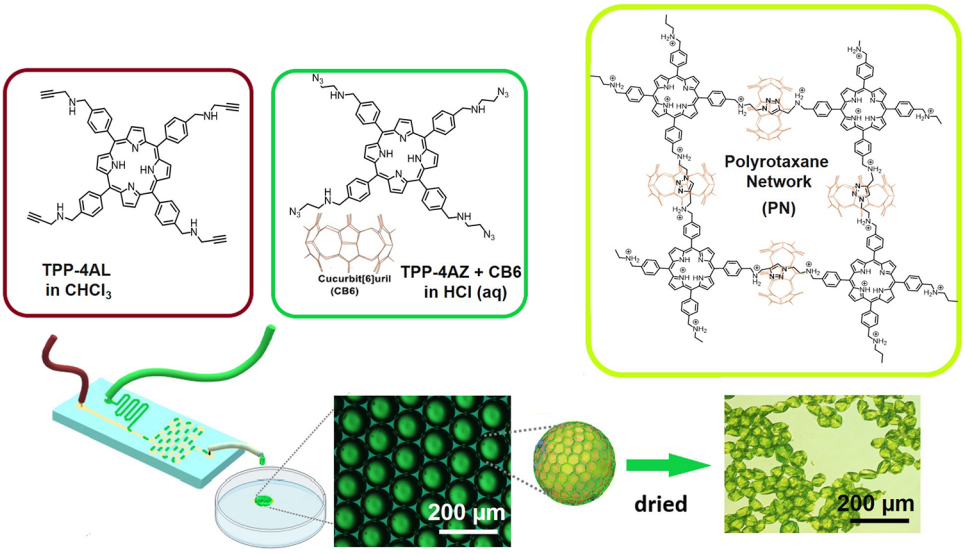

Figure 2. Schematic representation of the formation of PN microcapsules using a hydrophobic T-junction microfluidic chip through the CB6-AAC reaction between TPP-4AL in chloroform/hexadecane and TPP-4AZ, CB6 in aqueous HCl.

Zeiss Axio fluorescence microscope coupled with a digital Zeiss AxioCam MR Camera.

2.2. Fabrication of PN Microcapsules. A hydrophobic T-junction PDMS/glass microfluidic chip was used in this work to generate monodisperse water-in-oil microdroplets. The width and height of all channels were 150 and 80 μm, respectively. The length of the continuous phase, dispersed phase, and main channel were 1, 18, and 3 cm, respectively. Aqueous droplets were formed inside the hydrophobic oil phase using a pressure controller. Using a single-pressure source and bifurcation, microchannel inlet pressures for both continuous and dispersed phases were set as identical at 60 mbar. The single-pressure source configuration is schematically shown in Figure 1. Here, the oil and aqueous phases were prepared using the same methods reported in our previous paper.[1] Briefly, the oil phase was obtained by dissolving TPP-4AL (2.2 mg, 2.5 μmol) in 10 mL of chloroform. The aqueous phase was prepared by separately dissolving TPP-4AZ (2.5 mg, 2.5 μmol) and CB6 (10 mg, 10 μmol) in 5 mL of 1 M HCl followed by mixing of the two solutions for 5 min to obtain 10 mL of the homogeneous aqueous solution. The continuous phase was prepared by diluting the oil phase with hexadecane (1:4 v/v) followed by dissolving 2% Span80 surfactant. The dispersed phase was obtained by diluting the aqueous phase with water (1:4 v/v). Both the continuous and dispersed phases were then sonicated for 5 min at RT (room temperature) using the ultrasonic bath. Initially, the continuous oil phase was pumped into the microfluidic device to wet the microchannels. The aqueous dispersed phase was then injected through the other input channel of the T-junction device with the same applied pressure as the continuous phase. Microdroplet formation was achieved in the dripping phase, and the resultant droplets were collected in a Petri dish for further investigation using a tubing attached to the outlet. The monodisperse supramolecular microcapsules were capable of encapsulating the desired macromolecular cargos.

2.3. Encapsulation of Rhodamine 6G (Rh6G) Dye as a Cargo Molecule. Rh6G-loaded PN microcapsules were fabricated as follows: First, the aqueous and the oil phases were prepared as described in Section 2.2. Then, the dispersed phase was obtained by diluting the aqueous phase (TPP-4AZ and CB6 in HCl 1 M) with 200 ppm aqueous solution of Rh6G dye (1:4 v/v). The continuous phase was also prepared by diluting the oil phase (TPP-4AL in chloroform) with hexadecane (1:4 v/v) followed by adding 2% Span80 surfactant. Both the dispersed and continuous phases were sonicated for 5 min at RT using the ultrasonic bath, and then they were injected into the T-junction microfluidic chip through the same source of a pressure-control system using the optimized microfluidic droplet generation technique and the same microfluidic configuration. The resulting extra-monodisperse Rh6G-loaded PN microdroplets at the junction were carried to the Petri dish substrate through flexible tubing to study the releasing behavior of the Rh6G dye serving as a cargo molecule inside the PN microcapsules.

3. RESULTS AND DISCUSSION

3.1. Fabrication and Characterizations of PN Microcapsules. In this study, an optimized microfluidic droplet generation technique in combination with the interfacial polymerization to synthesize the catalytically self-threading polyrotaxane network (PN) was applied for direct generation of the monodisperse water-in-oil PN microdroplets. To minimize the external and internal fluctuations in the droplet generation process, a highly engineered channel network design and flow source configuration were applied to produce the ultra-monodisperse droplets with CVs of less than 0.2%. Supplying the inlet pressures from the same source along with similar hydrodynamic resistances of the inlet channel allow for minimum pressure difference between the two solutions at the junction. Low interfacial tension and low hydrodynamic resistance of the main channel are also applied to achieve ultrahigh monodispersity. The single-pressure source configuration in comparison with the traditional microfluidic system is shown in Figure 1. Unlike the traditional method in which two separate pressure sources/channels are used to supply the immiscible phases in the inlet channels, here, only one pressure source is used to supply the solutions. A T-shaped bifurcation is used to divide the air flow from a single air supply into two branches, and each of the branches is then used to drive one of the two immiscible phases. Also, the hydrodynamic resistances of the inlet channels are adjusted to be identical, and the interfacial tension is lowered using a surfactant. These design factors diminish the pressure difference at the junction between the two solutions. Furthermore, the hydrodynamic resistance of the main channel is decreased by using a shorter outlet channel. The flow rates of dispersed and continuous phases can be adjusted by inlet channel hydrodynamic resistances.[35]

The molecular structures of the monomers and the target PN as well as the hydrophobic microfluidic T-junction chip to

https://doi.org/10.1021/acsapm.2c00195
ACS Appl. Polym. Mater. 2022, 4, 4681−4688

construct PN microcapsules are shown in Figure 2. Target PN and its monomers (TPP-4AL, TPP-4AZ, and CB6) were synthesized and characterized according to the procedures reported in our previous paper.[1,6] The oil phase containing TPP-4AL (1 equimolar) and the aqueous phase containing TPP-4AZ (1 equimolar) and CB6 (4 equimolar) were prepared following the procedures[1] described in Section 2.2. The solution of 1:4 v/v TPP-4AL in chloroform and hexadecane was injected to one inlet to be used as the continuous phase, while the aqueous solution of 1:4 v/v TPP-4AZ and CB6 in 1 M HCl and water was used as the dispersed phase. Both continuous and dispersed phases were injected into the microfluidic chip through a pressure-controlled system. Microdroplets were generated at the junction and with the aid of flexible tubing; they were transferred to the Petri dish where the formation of PN was completed at the surface of the droplet,s and the microcapsules were obtained. The target PN was self-assembled through the water−oil interfacial polymerization between the oil and aqueous phases containing functionalized porphyrin monomers and CB6. Here, CB6 accelerates the 1,3-dipolar azide−alkyne cycloaddition reaction (CB6-AAC)[1,6,9,23] between TPP-4AZ and TPP-4AL to yield triazoles, which are encapsulated in the cavity of CB6 and, after cycloaddition CB6, remains as a part of the polyrotaxane network (PN).

The resulting spherical PN microcapsules exhibited a high level of monodispersity with a mean diameter of approximately 100 μm upon collecting them on the Petri dish substrate (t = 0 min). Figure 3a−d shows the optical and confocal laser

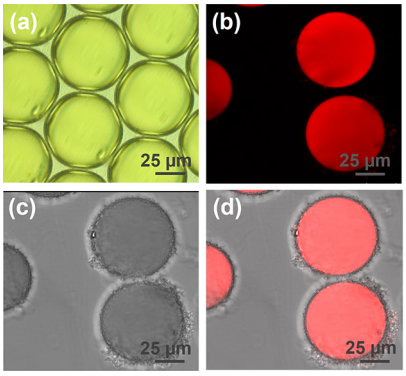

Figure 3. (a) Optical and (b−d) CLSM images of fresh PN microcapsules captured 5 min after generation: (b) fluorescence microscopy, (c) brightfield, and (d) overlaid representation.

scanning microscopy (CLSM) images of the fresh PN microcapsules captured 5 min after generation, which demonstrate that PN microcapsules have smooth spherical surfaces with a mean diameter of 65−70 μm (at t = 5 min).

The changes of the PN microcapsules over time was studied using fluorescence microscopy, and the results were presented in Figure 4. By evaporation of the inner aqueous phase of the microdroplets at room temperature during the first 15 min, their diameter continuously decreased with a slight distortion in the spherical shape. This is due to the weakening of the bonds in the interface, which form the stable microdroplet shell. Further evaporation led to the wrinkling of the flexible shell until the droplet was unable to support the microcapsule shell and subsequently resulted in complete collapse of the shell on the base substrate once it was dry.

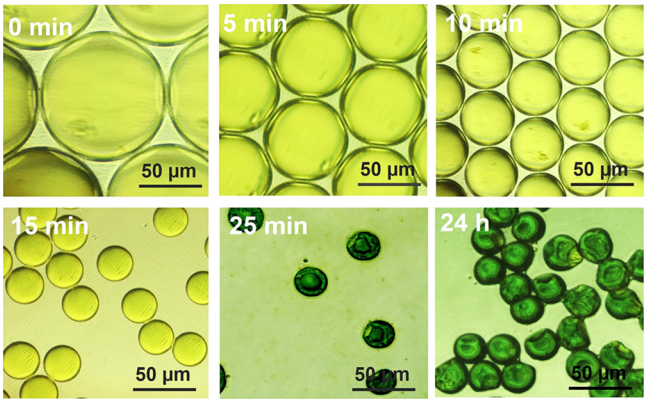

Figure 4. Fluorescence microscopy images (brightfield filter) of the formation of PN microcapsules as the water inside the microdroplets evaporates over time.

Figure 5 compares the fluorescence microscopy images (rhodamine filter) of fresh and air-dried PN microcapsules.

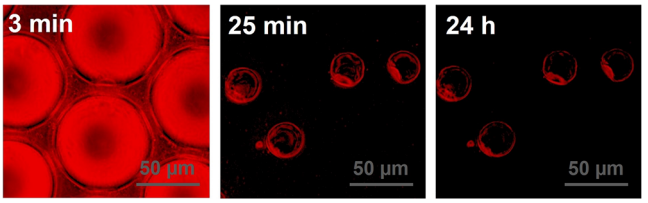

Figure 5. Fluorescence microscopy images (rhodamine filter) of the formation of PN microcapsules shells as the water inside the microdroplets evaporates.

The imaging revealed that the porphyrin-induced fluorescent red color was uniformly distributed all over the fresh droplets; however, with the gradual evaporation of the water inside the microdroplets, the red color was primarily observed on the surface of the microcapsules instead of the total volume of the droplets. This clearly confirmed that the interfacial polymerization of the oil and aqueous phases containing porphyrin monomers and CB6 to produce PN microcapsules was successful.

Microdroplets formed using the same conditions but in the absence of CB6 led to the formation of unstable microcapsules that collapsed as they merged, and then they gradually disappeared (Figure S1). This control experiment exclusively demonstrated the important role of CB6 to form the interfacial PN assembly because TPP-4AL and TPP-4AZ were no longer polymerized at the microdroplet surface in the absence of CB6. PN formation will also not take place in the presence of CB7 and CB8 because they are not capable of catalyzing 1,3-dipolar cycloaddition to form triazole by joining the monomers TPP-4AL and TPP-4AZ together.[1,9]

The rehydration of the air-dried PN microcapsule was also studied at room temperature. The fluorescence microscopy images showing the rehydration behavior of PN microcapsules over time were displayed in Figure 6. For this, 20 μL of water was injected into the Petri dish, which was then gradually absorbed by the dry PN microcapsules, and as a result of this, the dried microcapsules swelled gradually for the first few minutes to about 1.5 times the size of their dried state. After that, the PN microcapsules resumed their spherical shape, and the wrinkles disappeared from their shell. The rehydrated PN

https://doi.org/10.1021/acsapm.2c00195
ACS Appl. Polym. Mater. 2022, 4, 4681−4688

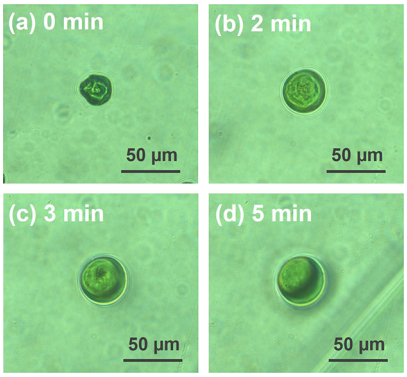

Figure 6. Fluorescence micrographs (brightfield filter) of one PN microcapsule: (a) air-dried and (b–d) after rehydration with water over time.

microcapsules were stable until the evaporation of the inner water phase of the microdroplets.

The surface morphology of the PN microcapsule samples was examined using the SEM. At first, a drop of the microcapsule dispersion was placed on a silicon wafer, dried in RT, and then sputtered with a 10 nm Au/Pd layer. Figure 7a,b shows the SEM images of dry PN microcapsules having

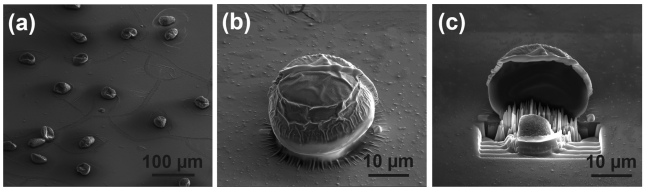

Figure 7. (a, b) SEM images and (c) FIB-SEM cross-sectional image of the dry PN microcapsules.

creases and folds on the flexible PN surface. To observe the internal structure of the PN microcapsule, a selected sample was FIB-milled to expose the microcapsule interior. Before milling, a 1 μm Pt layer was deposited on the surface of the samples. Figure 7c exhibits the cross-sectional FIB-SEM image of the dry PN microcapsule where the core-shell structure of these microcapsules was clearly observed.

To measure the shell thickness of the PN microcapsules, TEM imaging was used. First, a strip containing PN microcapsule layers (with a thickness of around 1.5 μm) was obtained by FIB milling. This strip was then transferred to a 3 mm TEM Cu grid using an Omniprobe micromanipulator. After attaching the sample using Pt deposition, the Omniprobe was detached from the strip. Figure 8 exhibits the cross-sectional TEM image of the resulting strip, which was composed of a 20 nm PN shell layer, a 10 nm Au layer, and a 1 μm Pt layer as well as the core.

The detailed compositional profiling of the same strip was investigated through TEM-EDX analysis. EDX analysis was used in line scan mode across the selected core-shell area of the PN strip as indicated by a red line in the corresponding cross-sectional HAADF STEM image (Figure 9a). Based on the elemental profiles displayed in Figure 9b and the corresponding atomic percentages of the elements (Table S1, ESI), the shell layer with a thickness of 20 nm comprising 78.80% C, 20.54% O, and 0.64% N, showed a distinct promotion of N and O content in the direction from core to shell. These observations clearly confirmed the successful formation of the

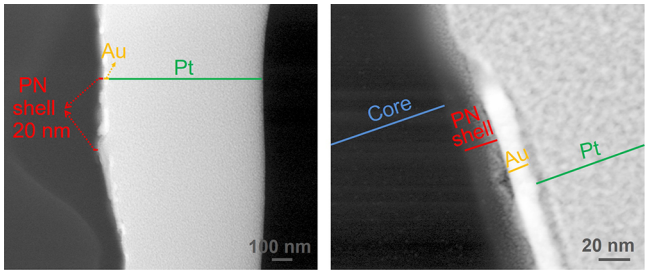

Figure 8. Cross-sectional TEM images of the PN microcapsule strip.

interfacial PN assembly at the microcapsule shell through the interfacial polymerization between the aqueous and oil phases.

3.2. Release of the Entrapped Rhodamine 6G (Rh6G) Cargo Molecules from the PN Microcapsules. The specifically prepared microcapsules can entrap molecular guests as drug molecules for drug delivery or enzyme/molecular catalysis to catalyze the reactions as well as acting as a microvessel to carry out specific reactions. Here, we want to demonstrate the proof-of-concept application for encapsulating and releasing small molecules as drug substitutes. To this end, the fluorescent Rh6G dye, as a cargo molecule, was encapsulated inside the PN microcapsules using the procedure described in Section 2.3. Here, the Rh6G cargo was added to the dispersed aqueous phase, and it was entrapped inside the microdroplets during their generation process through the optimized microfluidic droplet generation technique as mentioned before. The resulting extra-monodisperse microdroplets were then transferred to the Petri dish substrate. The monodisperse PN microcapsules containing entrapped Rh6G were generated after the interfacial assembly of the polyrotaxane network at the droplet interface and monitored over time by a fluorescence microscope under a rhodamine filter to investigate the releasing behavior of the Rh6G cargo from the PN microcapsule in dry medium. As shown in Figure S2, the color of the fresh PN microcapsules was uniformly red, whereas by gradual evaporation of the water inside of them over time, the red-colored microcapsules turned green, illustrating the encapsulation of the Rh6G cargo inside the fresh PN microcapsules and its continuous release over time. There, the size of the Rh6G-loaded PN microcapsules was continuously decreased over time due to the evaporation of their inner aqueous phase. To quantify the release of the Rh6G cargo from the PN microcapsules, the captured optical images were analyzed with ImageJ image-processing software. For this, the mean fluorescence intensity from the interior of the microcapsules was calculated for all images by averaging the pixel intensity inside the microcapsule and subtracting the background intensity (measured close to the microcapsule) using the software. Figure S3 exhibits the release profile of the Rh6G dye from the PN microcapsules in dry medium, in which 67% of the cargo was released over 1 h.

To study the releasing behavior of the Rh6G cargo from the PN microcapsules in aqueous medium, the Rh6G-loaded PN microcapsules were first generated as described in Section 2.3, and then approximately 5 min after their generation, they were transferred to the Petri dish substrate containing water and tracked over time by the fluorescence microscope under a brightfield filter. The release profile of Rh6G dye from the PN microcapsules was obtained by analyzing 129 optical images taken over 7 h. Figure 10a–f shows the optical images of the Rh6G-loaded PN microcapsules taken during this study. Figure

https://doi.org/10.1021/acsapm.2c00195
ACS Appl. Polym. Mater. 2022, 4, 4681–4688

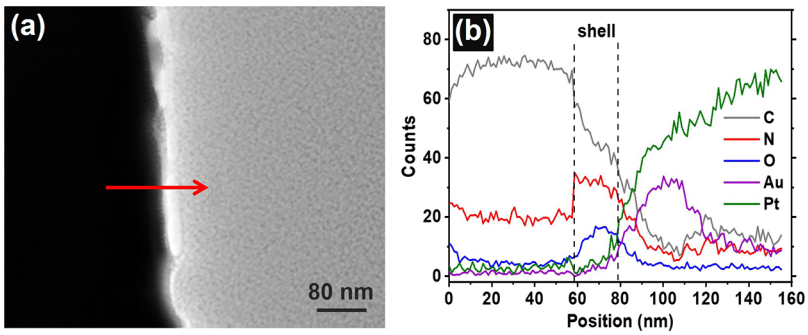

Figure 9. (a) HAADF STEM image and (b) TEM-EDX line scan profile of the selected cross section of the core-shell area of the PN microcapsule strip.

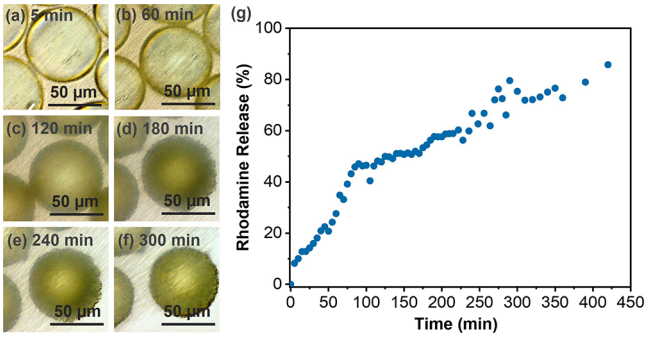

Figure 10. Release of Rh6G dye from the PN microcapsules inside the water: (a–f) fluorescence micrographs (brightfield filter) of the Rh6G-loaded PN microcapsules, demonstrating the release of Rh6G cargo in the water, and (g) the release profile of the Rh6G dye from the PN microcapsules over 420 min.

10g demonstrates the corresponding long-term release profile of the Rh6G-loaded PN microcapsules inside the water. As can be derived from Figure 10, the Rh6G cargo was gently released from the PN microcapsules inside the water over 7 h and no significant change in the size and shape of the microcapsules was observed. Here, only 28% of the Rh6G cargo released over the first 1 h, and then it reached to 48% over 2 h and 86% after 7 h. Compared with the release experiment performed in dry medium, the release rate of the Rh6G cargo from the PN microcapsules in aqueous medium (Figure 10g) was much slower than those in dry medium (Figure S3). The obtained results ensured that the controlled cargo release lasted for the target duration.

4. CONCLUSIONS

High-monodispersity droplet generation methodology has been used for the first time in microcapsule synthesis, specifically for polyrotaxane–based supramolecular microcapsules. Combining the distinctive liquid–liquid interfacial polymerization method and the unique microfluidic droplet generation technique, highly monodisperse supramolecular microcapsules were prepared. To obtain extremely monodisperse droplets, only one port of pressure source was applied to drive both inlet phases, the interfacial tension was diminished using a surfactant, and the main-channel hydrodynamic resistance was designed to be low. The CB6-AAC reaction between TPP-4AZ and TPP-4AL at the water and the oil phase interfaces resulted in the self-assembly of the target polyrotaxane network (PN) with a thickness of 20 nm on the surface of the ultra-monodisperse microdroplets. The resulting water-in-oil PN microcapsules offer high monodispersity, ability to retain target molecules, and facilitation of release via supramolecular cross-links. Moreover, the release rate of the Rh6G cargo from the PN microcapsules inside the aqueous medium was investigated over time for controlled drug release applications. The results demonstrated the long-term cargo release profile for the Rh6G-loaded PN microcapsules without any significant change in the size and shape of the PN microcapsules, in which the Rh6G was gradually released from the PN microcapsules inside the water during 7 h. The versatile process presented in this work can be utilized to produce nano- or microcapsules for controlled cargo release applications.

■ ASSOCIATED CONTENT

Supporting Information

The Supporting Information is available free of charge at https://pubs.acs.org/doi/10.1021/acsapm.2c00195.

(Figures S1–S3) Fluorescence microscopy images (brightfield filter) of the formation of the PN microcapsules in the absence of CB6 over time; fluorescence microscopy images (rhodamine filter) of the Rh6G-loaded PN microcapsules as the water microdroplet evaporates over time; release profile of the Rh6G dye from the PN microcapsules over time on the dry Petri dish substrate; (Table S1) atomic percentage of the constituent elements of the dry PN microcapsule strip obtained from the TEM-EDX line scan (PDF)

■ AUTHOR INFORMATION

Corresponding Authors

Caglar Elbuken – *Institute of Materials Science and Nanotechnology, National Nanotechnology Research Center (UNAM), Bilkent University, Ankara 06800, Turkey; Faculty of Biochemistry and Molecular Medicine, Faculty of Medicine, University of Oulu, 90014 Oulu, Finland;* orcid.org/0000-0001-8359-6871; Email: celbuken@gmail.com

Dönüs Tuncel – *Institute of Materials Science and Nanotechnology, National Nanotechnology Research Center (UNAM) and Department of Chemistry, Bilkent University, Ankara 06800, Turkey;* orcid.org/0000-0001-7762-9200; Email: dtuncel@fen.bilkent.edu.tr

Authors

Elnaz Alizadeh-Haghighi – *Institute of Materials Science and Nanotechnology, National Nanotechnology Research Center (UNAM), Bilkent University, Ankara 06800, Turkey*

https://doi.org/10.1021/acsapm.2c00195
ACS Appl. Polym. Mater. 2022, 4, 4681–4688

Aisan Khaligh − *Institute of Materials Science and Nanotechnology, National Nanotechnology Research Center (UNAM) and Department of Chemistry, Bilkent University, Ankara 06800, Turkey;* orcid.org/0000-0002-5419-1020

Ali Kalantarifard − *Institute of Materials Science and Nanotechnology, National Nanotechnology Research Center (UNAM), Bilkent University, Ankara 06800, Turkey; Faculty of Biochemistry and Molecular Medicine, Faculty of Medicine, University of Oulu, 90014 Oulu, Finland*

Complete contact information is available at: https://pubs.acs.org/10.1021/acsapm.2c00195

Author Contributions

#E.A.-H. and A. Khaligh contributed equally to this work.

Author Contributions

D.T. and C.E. conceived the idea and supervised and coordinated the project. D.T., C.E., E.A.-H., and A. Khaligh designed the experiments. E.A.-H. and A. Kalantarifard performed chip fabrication and microfluidic setup optimization. A. Kalantarifard carried out the initial experiments of PN microcapsule formation and performed optical image analysis using ImageJ software. E.A.-H. and A. Khaligh optimized the PN microcapsules, performed all related experiments, dye release, fluorescent and CLSM microscopy observations, and data analysis. A. Khaligh synthesized and characterized CB6, TPP-4AL, TPP-4AZ, PN, and all of the organic precursors as well as contributed for the cross-sectional TEM imaging and TEM-EDX data analysis of the microcapsules. A Khaligh. and E.A.-H. wrote the manuscript. C.E. and D.T. revised the manuscript. All authors have given approval to the final version of the manuscript. There authors declare no competing financial interest.

Notes

The authors declare no competing financial interest.

■ ACKNOWLEDGMENTS

This work was partially supported by the Academy of Finland, NanoEngineered Self-Assembling Vesicle Production Line (NESAV) project grant no. 342448 and The Scientific and Technological Research Council of Turkey-TÜBİTAK (KBAG 114Z0195).

■ ABBREVIATIONS

SEM, scanning electron microscopy; TEM, transmission electron microscopy; FIB, focused ion beam; EDX, energy-dispersive X-ray spectroscopy; CLSM, confocal laser scanning microscopy; PN, 2D-polyrotaxane network; TPP-4AL, tetra propyl amine functionalized porphyrin; TPP-4AZ, tetra azido amine functionalized porphyrin; CB6, cucurbit[6]uril; Rh6G, rhodamine 6G; RT, room temperature

■ REFERENCES

(1) Khaligh, A.; Khan, R.; Akolpoğlu Başaran, D. D.; Özkan, M.; Tuncel, D. Photoactive Catalytically Self-Threaded 2D Polyrotaxane Network for Visible Light Activated Antimicrobial Phototherapy. *ACS Appl. Polym. Mater.* **2020**, *2*, 5726−5734.

(2) Matsumoto, M.; Valentino, L.; Stiehl, G. M.; Balch, H. B.; Corcos, A. R.; Wang, F.; Ralph, D. C.; Mariñas, B. J.; Dichtel, W. R. Lewis-Acid-Catalyzed Interfacial Polymerization of Covalent Organic Framework Films. *Chem* **2018**, *4*, 308−317.

(3) Zheng, Y.; Yu, Z.; Parker, R. M.; Wu, Y.; Abell, C.; Scherman, O. A. Interfacial Assembly of Dendritic Microcapsules with Host−Guest Chemistry. *Nat. Commun.* **2014**, *5*, 1−9.

(4) Girek, B.; Sliwa, W. Noncovalent Assemblies of Cationic Porphyrins with Cage Macrocycles. *J. Inclusion Phenom. Macrocyclic Chem.* **2015**, *81*, 35−48.

(5) Liu, K.; Liu, Y.; Yao, Y.; Yuan, H.; Wang, S.; Wang, Z.; Zhang, X. Supramolecular Photosensitizers with Enhanced Antibacterial Efficiency. *Am. Ethnol.* **2013**, *52*, 8285−8289.

(6) Tuncel, D.; Cindir, N.; Koldemir, Ü. [5] Rotaxane and [5] Pseudorotaxane Based on Cucurbit[6]uril and Anchored to a Meso-tetraphenyl Porphyrin. *J. Inclusion Phenom. Macrocyclic Chem.* **2006**, *55*, 373−380.

(7) Zhang, C.-C.; Liu, X.; Liu, Y.-P.; Liu, Y. Two-Dimensional Supramolecular Nanoarchitectures of Polypseudorotaxanes Based on Cucurbit[8]Uril for Highly Efficient Electrochemical Nitrogen Reduction. *Chem. Mater.* **2020**, *32*, 8724−8732.

(8) Xue, M.; Yang, Y.; Chi, X.; Yan, X.; Huang, F. Development of Pseudorotaxanes and Rotaxanes: from Synthesis to Stimuli-Responsive Motions to Applications. *Chem. Rev.* **2015**, *115*, 7398−7501.

(9) Tuncel, D.; Ünal, Ö.; Artar, M. Supramolecular Assemblies Constructed by Cucurbituril-Catalyzed Click Reaction. *Isr. J. Chem.* **2011**, *51*, 525−532.

(10) Sauvage, J. P. From Chemical Topology to Molecular Machines (Nobel Lecture). *Am. Ethnol.* **2017**, *56*, 11080−11093.

(11) Sayed, M.; Pal, H. An Overview from Simple Host−Guest Systems to Progressively Complex Supramolecular Assemblies. *Phys. Chem. Chem. Phys.* **2021**, *23*, 26085−26107.

(12) Gürbüz, S.; Idris, M.; Tuncel, D. Cucurbituril-Based Supramolecular Engineered Nanostructured Materials. *Org. Biomol. Chem.* **2015**, *13*, 330−347.

(13) Kim, K. *Cucurbiturils and Related Macrocycles*, Royal Society of Chemistry: Cambridge 2019, DOI: 10.1039/9781788015967.

(14) Cheng, G.; Luo, J.; Liu, Y.; Chen, X.; Wu, Z.; Chen, T. Cucurbituril-Oriented Nanoplatforms in Biomedical Applications. *ACS Appl. Bio Mater.* **2020**, *3*, 8211−8240.

(15) Tang, B.; Zhao, J.; Xu, J. F.; Zhang, X. Cucurbit[n]urils for Supramolecular Catalysis. *Chem. - Eur. J.* **2020**, *26*, 15446−15460.

(16) D., Tuncel, *Cucurbituril-based Functional Materials*, Royal Society of Chemistry: Cambridge, 2019.

(17) Yang, D.; Liu, M.; Xiao, X.; Tao, Z.; Redshaw, C. Polymeric Self-Assembled cucurbit[n]urils: Synthesis, Structures and Applications. *Coord. Chem. Rev.* **2021**, *434*, 213733.

(18) Liu, J.; Tan, C. S. Y.; Scherman, O. A. Dynamic Interfacial Adhesion Through Cucurbit[n]uril Molecular Recognition. *Am. Ethnol.* **2018**, *130*, 8992−8996.

(19) Liu, J.; Tan, C. S. Y.; Yu, Z.; Lan, Y.; Abell, C.; Scherman, O. A. Biomimetic Supramolecular Polymer Networks Exhibiting Both Toughness and Self-Recovery. *Adv. Mater.* **2017**, *29*, 1604951.

(20) Khaligh, A.; Sheidaei, Y.; Tuncel, D. Covalent Organic Framework Constructed by Clicking Azido Porphyrin with Perpropargyloxy-Cucurbit[6]uril for Electrocatalytic Hydrogen Generation from Water Splitting. *ACS Appl. Energy Mater.* **2021**, *4*, 3535−3543.

(21) Zhang, Q.; Zhou, D.-D.; Zhang, J.-W.; Gao, D.; Yang, F.-Q.; Chen, H.; Xia, Z.-N. Amino-Terminated Supramolecular Cucurbit[6]-uril Pseudorotaxane Complexes Immobilized on Magnetite@Silica Nanoparticles: A Highly Efficient Sorbent for Salvianolic Acids. *Talanta* **2019**, *195*, 354−365.

(22) Finbloom, J. A.; Han, K.; Slack, C. C.; Furst, A. L.; Francis, M. B. Cucurbit[6]Uril-Promoted Click Chemistry for Protein Modification. *J. Am. Chem. Soc.* **2017**, *139*, 9691−9697.

(23) Özkan, M.; Keser, Y.; Hadi, S. E.; Tuncel, D. A [5]Rotaxane-Based Photosensitizer for Photodynamic Therapy. *Eur. J. Org. Chem.* **2019**, *2019*, 3534−3541.

(24) Berdimurodov, E.; Kholikov, A.; Akbarov, K.; Guo, L.; Kaya, S.; Katin, K. P.; Verma, D. K.; Rbaa, M.; Dagdag, O. Novel Cucurbit[6]Uril-Based [3]Rotaxane Supramolecular Ionic Liquid As a Green And Excellent Corrosion Inhibitor for the Chemical Industry. *Colloids Surf., A* **2022**, *633*, 127837.

(25) Bah, M. G.; Bilal, H. M.; Wang, J. Fabrication and Application of Complex Microcapsules: A Review. *Soft Matter* **2020**, *16*, 570−590.
(26) Wang, S.; Liu, H.; Wu, D.; Wang, X. Temperature and pH Dual-Stimuli-Responsive Phase-Change Microcapsules for Multipurpose Applications in Smart Drug Delivery. *J. Colloid Interface Sci.* **2021**, *583*, 470−486.
(27) Lee, T. Y.; Choi, T. M.; Shim, T. S.; Frijns, R. A.; Kim, S.-H. Microfluidic Production of Multiple Emulsions and Functional Microcapsules. *Lab Chip* **2016**, *16*, 3415−3440.
(28) Duncanson, W. J.; Lin, T.; Abate, A. R.; Seiffert, S.; Shah, R. K.; Weitz, D. A. Microfluidic Synthesis of Advanced Microparticles for Encapsulation and Controlled Release. *Lab Chip* **2012**, *12*, 2135−2145.
(29) Datta, S. S.; Abbaspourrad, A.; Amstad, E.; Fan, J.; Kim, S. H.; Romanowsky, M.; Shum, H. C.; Sun, B.; Utada, A. S.; Windbergs, M.; Zhou, S.; Weitz, D. A. Double Emulsion Templated Solid Microcapsules: Mechanics and Controlled Release. *Adv. Mater.* **2014**, *26*, 2205−2218.
(30) Weiss, M.; Frohnmayer, J. P.; Benk, L. T.; Haller, B.; Janiesch, J.-W.; Heitkamp, T.; Börsch, M.; Lira, R. B.; Dimova, R.; Lipowsky, R.; Bodenschatz, E.; Baret, J. C.; Vidakovic-Koch, T.; Sundmacher, K.; Platzman, I.; Spatz, J. P. Sequential Bottom-Up Assembly of Mechanically Stabilized Synthetic Cells by Microfluidics. *Nat. Mater.* **2018**, *17*, 89−96.
(31) Liu, J.; Lan, Y.; Yu, Z.; Tan, C. S.; Parker, R. M.; Abell, C.; Scherman, O. A. Cucurbit[n]uril-Based Microcapsules Self-Assembled within Microfluidic Droplets: A Versatile Approach For Supramolecular Architectures and Materials. *Acc. Chem. Res.* **2017**, *50*, 208−217.
(32) Wang, J. T.; Wang, J.; Han, J. J. Fabrication of Advanced Particles and Particle-Based Materials Assisted by Droplet-Based Microfluidics. *Small* **2011**, *7*, 1728−1754.
(33) Kim, J. W.; Utada, A. S.; Fernández-Nieves, A.; Hu, Z.; Weitz, D. A. Fabrication of Monodisperse Gel Shells and Functional Microgels in Microfluidic Devices. *Am. Ethnol.* **2007**, *119*, 1851−1854.
(34) Schloss, A. C.; Liu, W.; Williams, D. M.; Kaufman, G.; Hendrickson, H. P.; Rudshteyn, B.; Fu, L.; Wang, H.; Batista, V. S.; Osuji, C.; Yan, E. C. Y.; Regan, L. Fabrication of Modularly Functionalizable Microcapsules Using Protein-Based Technologies. *ACS Biomater. Sci. Eng.* **2016**, *2*, 1856−1861.
(35) Kalantarifard, A.; Alizadeh-Haghighi, E.; Saateh, A.; Elbuken, C. Theoretical and Experimental Limits of Monodisperse Droplet Generation. *Chem. Eng. Sci.* **2021**, *229*, 116093.
(36) Deng, N.-N.; Yelleswarapu, M.; Huck, W. T. Monodisperse Uni-and Multicompartment Liposomes. *J. Am. Chem. Soc.* **2016**, *138*, 7584−7591.
(37) Zhu, P.; Wang, L.Microfluidics-Enabled Soft Manufacture of Materials with Tailorable Wettability. *Chem. Rev.* **2021**, DOI: 10.1021/acs.chemrev.1c00530
(38) Zhang, G.; Sun, J. Lipid in Chips: A Brief Review of Liposomes Formation by Microfluidics. *Int. J. Nanomed.* **2021**, *16*, 7391.
(39) Yu, Z.; Lan, Y.; Parker, R. M.; Zhang, W.; Deng, X.; Scherman, O. A.; Abell, C. Dual-Responsive Supramolecular Colloidal Microcapsules From Cucurbit[8]uril Molecular Recognition in Microfluidic Droplets. *Polym. Chem.* **2016**, *7*, 5996−6002.
(40) Zhang, J.; Coulston, R. J.; Jones, S. T.; Geng, J.; Scherman, O. A.; Abell, C. One-Step Fabrication of Supramolecular Microcapsules from Microfluidic Droplets. *Science* **2012**, *335*, 690−694.
(41) Yu, Z.; Zhang, J.; Coulston, R. J.; Parker, R. M.; Biedermann, F.; Liu, X.; Scherman, O. A.; Abell, C. Supramolecular Hydrogel Microcapsules via Cucurbit[8]uril Host−Guest Interactions with Triggered and UV-Controlled Molecular Permeability. *Chem. Sci.* **2015**, *6*, 4929−4933.

https://doi.org/10.1021/acsapm.2c00195
ACS Appl. Polym. Mater. 2022, 4, 4681−4688